Ukrainian Journal of Physical Optics
ISSUE 3
2025

NEW SOLUTIONS FOR POLARIZATION-SENSITIVE OPTICAL COHERENCE TOMOGRAPHY

O.V. ANGELSKY[1,2], C.YU. ZENKOVA[2], A.YA. BEKSHAEV[3], D.I. IVANSKYI[2], M. DIACHENKO[4], JUN ZHENG[1*], XINZHENG ZHANG[5]

[1] Taizhou Research Institute of Zhejiang University, Taizhou City, Zhejiang Province, 318000 China
[2] Chernivtsi National University, 2 Kotsyubinsky Str., Chernivtsi 58012, Ukraine
[3] Physics Research Institute, Odesa I.I. Mechnikov National University, 2 Dvorianska, Odesa 65082, Ukraine
[4] Municipal Enterprise Chernivtsi Regional Clinical Cardiological Center, Chernivtsi, Ukraine
[5] The MOE Key Laboratory of Weak-Light Nonlinear Photonics and International Sino-Slovenian Joint Research Center on Liquid Crystal Photonics, TEDA Institute of Applied Physics and School of Physics, Nankai University, Tianjin 300457, China
*Corresponding author: dbzj@netease.com

Received: 14.05.2025

Abstract. The work is a development of the studies presented in [1] on the reconstruction of the corneal structure of the eye, using a modified Mach-Zehnder interferometer, equipped with a polarization modulator and a feedback loop. A distinctive feature of this approach is the consideration of the depolarization of the object signal, which arises due to scattering on epithelial cells and keratocytes of the cornea. The introduced ratio of polarized and depolarized intensities enabled the evaluation of the depolarization effect on the object signal, while the proposed experimental solution allowed for an increase in the accuracy of eye structure reconstruction by 22.84%. Elimination of the "noise" vertical component of the object signal, caused by the depolarization of the input horizontally linearly polarized wave, led to the successful reconstruction of the corneal structure from the vertical channel of the interferometer, as demonstrated in this study.

Keywords: optical coherence tomography, depolarization, scattering centers, birefringence, Monte-Carlo method, Mach-Zehnder interferometer
UDC: 535.4, 535.5
DOI: 10.3116/16091833/Ukr.J.Phys.Opt.2025.03067

1. Introduction

This study builds upon previous work [1] on corneal structure reconstruction using polarization-sensitive optical coherence tomography (PS-OCT) by analyzing dynamic and geometric phase information obtained from interference patterns in the vertical and horizontal channels of a Mach–Zehnder interferometer.

PS-OCT allows detection of polarization changes caused by birefringent biological structures [2-6]. Traditional PS-OCT methods face limitations in interpreting the object signal when analyzing the birefringent properties of biological samples because scattered light information accumulates in the signal. As a result, signal depolarization greatly reduces the method's sensitivity, lowers resolution, image contrast, and diagnostic quality [7-12].

One method for reducing the effects of signal depolarization and improving measurement accuracy was proposed in [13], using an approach that averages multiple Jones matrix volumes measured at different focal positions.

Nevertheless, the actual search for experimental and model-based solutions remains to simultaneously restore the structure of a birefringent, transparent (translucent) biological

object both in volume and in the underlying thin layers with high accuracy, identify the localization of scattering centers, and, as a result, eliminate the depolarization of the object's signal throughout the depth of longitudinal scanning of the sample.

2. Degree of polarization estimation within the Monte Carlo approach

To fully describe the structure of the eye using the new PS-OCT solutions, it is necessary to consider all possible physical mechanisms that influence how incident light interacts with the structural layers responsible for forming the resulting interference pattern in the interferometer channels. Building on the results of [1] regarding absorption in different layers of the cornea and the presence of birefringence in the lamellae—reproduced in several of our works [14-17]—this study also accounts for scattering centers as *sources of depolarization* of the incident horizontally linearly polarized beam. We expand the theoretical framework by employing a Monte Carlo-based model that includes *depolarization effects* caused by scattering. Accordingly, a novel solution is proposed based on an experimental setup utilizing a Mach–Zehnder interferometer.

When modeling the beam that contributes to forming an object signal with information about the structure of stromal lamellae, the presence of distributed keratocytes in the stroma is assumed to account for the depolarization of radiation caused by scattering in the epithelium. Depolarization of radiation does not occur in scattering on keratocytes. The beam incident on the eye cornea is characterized by a Gaussian intensity distribution, the half-width of which corresponds to the diameter of the beam waist in the focal plane $2w_f = 7.15$ μm. Let us assume a focal depth of the beam b = 100 μm. In the framework of modeling the depolarization of the object beam, we estimate $I_{\parallel}$ and $I_{\perp}$ for the beam in the forward (backward) directions at the corresponding channels of the interferometer. The total parallel or perpendicular components are obtained as the integral value of projections over all polarization azimuths and represent the area under a conceptual histogram of the appropriate distribution.

For single scattering, depolarization is practically absent, with only the polarization state changing, then for multiple scattering, partial depolarization of the photon packet can occur [18].

To estimate the degree of polarization, we use the Stokes parameters of the *i*-th photon packet, i.e., we write

$$I_i = E_{\parallel i}E^*_{\parallel i} + E_{\perp i}E^*_{\perp i}, Q_i = E_{\parallel i}E^*_{\parallel i} - E_{\perp i}E^*_{\perp i}, U_i = E_{\parallel i}E^*_{\perp i} + E_{\perp i}E^*_{\parallel i}, V_i = i\left(E_{\parallel i}E^*_{\perp i} - E_{\perp i}E^*_{\parallel i}\right). \quad (1)$$

Accordingly, the Stokes parameters for the optical field, taking into account W_i – the weight of the *i*-th photon packet and N – the number of photon packets, can be represented as

$$I = \frac{1}{N}\sum_{i=1}^{N} W_i I_i, \quad Q = \frac{1}{N}\sum_{i=1}^{N} W_i Q_i, \; U = \frac{1}{N}\sum_{i=1}^{N} W_i U_i, \; V = \frac{1}{N}\sum_{i=1}^{N} W_i V_i. \quad (2)$$

Taking into account ($I_{\parallel}$) and cross- ($I_{\perp}$) polarized intensity light for linearly polarized radiation, the degree of polarization [18]: $P = \left[I_{\parallel} - I_{\perp}\right] / \left[I_{\parallel} + I_{\perp}\right]$ For example, if $N \sim 10^4$, then $P = 0.73$, i.e., with a probability of 73%, we can assume that the radiation that hits the subsequent layers will remain linearly polarized.

For a partially polarized field, the degree of polarization is given by $P=\frac{\sqrt{Q^2+U^2+V^2}}{I}$. When averaging over the beam cross section, the Stokes vector is expressed in terms of its fully polarized and unpolarized components [19,20]:

$$S=\begin{pmatrix} I \\ Q \\ U \\ V \end{pmatrix}=S_{pol}+S_{unp}=P\begin{pmatrix} I \\ Q/P \\ U/P \\ V/P \end{pmatrix}+(1-P)\begin{pmatrix} I \\ 0 \\ 0 \\ 0 \end{pmatrix}. \quad (3)$$

Then for the selected beam parameters, for the forward direction, the intensity components are: $I_{\|}=0.864$, $I_{\perp}=0.136$, which corresponds to the degree of linear polarization $P=0.73$, the ratio of polarized and depolarized intensities [21] $I_{\|}/I_{\perp}=6.35$. For the backward direction, respectively $I_{\|}=0.71$, $I_{\perp}=0.29$, $P=0.42$, $I_{\|}/I_{\perp}=2.45$. According to [21], the degree of polarization depends on medium depth d as: $P(d)\cong[3/2]\times\exp(-d/l_p)$, where l_p is the depolarization length. By fitting data points calculated by the Monte Carlo (MC) method: $P(d)=1.29\exp(-d/l_p)$. Obtaining the value of P from both dependencies at individual discrete points (depths), taking into account that $P=[I_{\|}-I_{\perp}]/[I_{\|}+I_{\perp}]$, allows for the reconstruction of $I_{\|}$ and $I_{\perp}$, and thus the estimation of the ratio of polarized and depolarized intensities.

The curve of the ratio of polarized and depolarized intensities for the theoretical dependence (Fig. 1, blue curve) has an analytical form: $I_{\|}/I_{\perp}=1.33+[1.36\times10^6/d^3]$, and the one obtained by the MC method (Fig. 1, yellow curve): $I_{\|}/I_{\perp}=1.01+[1.35\times10^4/d^2]$.

The theoretical and model-based values of the ratio of polarized and depolarized intensities differ only slightly when exiting the epithelium back (d=100 μm). A special value of the given dependencies is the layer thickness when $I_{\|}/I_{\perp}$ up to 2 [22], which enables the determination of the depolarization length l_p, according to Fig. 1 this thickness is approximately 117 μm, which exceeds the total thickness of the epithelium in both forward and backward directions (100 μm).

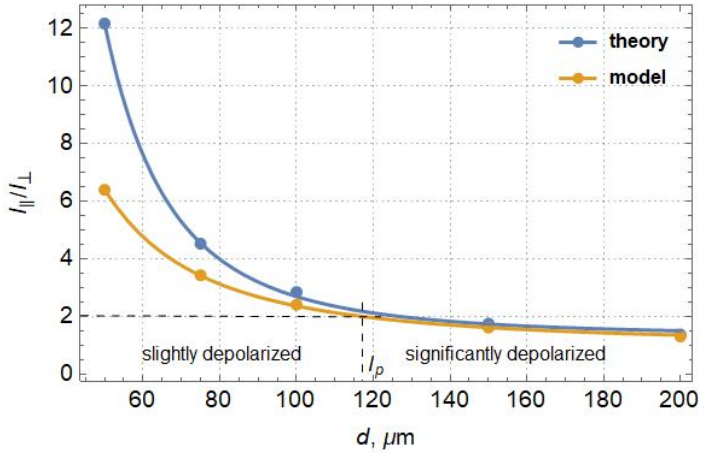

Fig. 1. The ratio of polarized and depolarized intensities with thickness. The theoretical dependence is represented by the blue line, while the yellow line shows the MC method results.

For a given value (117 μm) of the depolarization length l_p, the degree of polarization can be determined as P=0.33. This means that 67% of the radiation is depolarized. The discrete distribution of photons allows for the identification of the influence of depolarization on the level of useful, object signal during corneal scanning. Thus, the discrete points where the signal is evaluated are associated with pixels of the photosensitive matrix of the camera used [23], which involves averaging the degree of depolarization within a pixel, or using nanoaperture arrays with an aperture diameter of 10 nm [23], and enables to perform practically photon-by-photon scanning.

The consideration of depolarization in the object signal involves an algorithm that includes the calculation of the Stokes vector over the entire field based on pixel-by-pixel information, estimating the degree of polarization P of the beam, and evaluating both the polarized (S_{pol}) and unpolarized (S_{unp}) components of the Stokes vector for the given object beam. The parameters of the polarization ellipse can be determined through the polarized component of the Stokes vector, and then the information of the orthogonal linearly polarized components of the object beam $I_{\parallel,\perp} = \left[PI \pm Q\right]/2$ and the phase difference between orthogonal components $\tan\Delta\varphi_{ob} = V/U$ can be extracted. The degree of polarization (ratio of polarized and depolarized intensities) are determined by the intensity of the orthogonal components $I_{\parallel,\perp}$, but not the phase difference, which allows for analyzing and minimizing the effect of depolarization on the object signal, thus improving the signal-to-noise ratio, enhancing the accuracy of lamella structure reproduction, and the position of keratocytes. It should be noted that the vertical component of the polarization ellipse, associated with $I_{\perp}$, is formed only by birefringence in the lamella, without the influence of scattering or other effects at the interface that also affect the degree of polarization. Signal processing methods that utilize artificial intelligence (AI) and machine learning (ML) technologies lessen the impact of background signals caused by radiation depolarization.

The result of such processing will be a horizontally linearly polarized photon packet, which interacts with each subsequent lamella. The generation of linear polarization involves using an optical system in the probing beam (such as a QWP-HWP combination [24] or a Berek compensator [25]), the control of which is managed by an adapted intelligent technology enabling the creation of arbitrary polarization states. Then, with known parameters of depolarization in the epithelium and the anisotropy of the corresponding lamella, the polarization of the probing beam is modeled so that a horizontally linearly polarized beam falls on each lamella.

The proposed approach enables pixel-wise estimation of the ratio of polarized and depolarized intensities within the beam aperture, assuming that the detector consists of submicron-sized photosensitive pixels. This allows the extraction of the useful signal, i.e., the horizontal (polarized) component, for each pixel of the aperture. In contrast to conventional PS-OCT solutions, where the recording element is associated with the beam cross-section and the ratio of polarized and depolarized intensities is estimated by averaging the Stokes vector over the entire aperture, our proposed solution demonstrates an increase in transverse resolution in terms of depolarization contrast. Moreover, it also enhances the longitudinal resolution for thin surface layers diagnostics up to 100 nm, increasing the accuracy of stromal structure reconstruction. This possibility is realized only under the

condition of horizontal linear polarization of the incidence beam on the lamella, which is ensured by incorporating an additional polarization modulator (PM) introduced into the horizontal interferometer channel and a feedback line. Consequently, the vertical channel contains exclusively useful information about the structure (geometric and optical properties) of the object. Depolarization causes the appearance of a vertical "noise" component (both in the forward and backward directions) and forms a "noise" contribution to the useful signal at the level of 22.84%. Therefore, the removal of this component from the object beam, with the allocation of a pure "useful" signal in the vertical channel, corresponds to an increase in the accuracy of stromal structure reconstruction to 22.84%.

The object signal obtained after computer processing interacts with the reference beam.

3. Modified PS-OCT scheme and reconstructed structure of the object of study

The OCT signal is the result of the interaction of each individual photon packet with the reference wave. Let N_d photon packets be involved in the formation of the OCT signal, which is then analyzed to reconstruct of information about the object of study. The total interference signal from all photon packets is recorded within one pixel of 0.5 μm×0.5 μm.

To eliminate the influence of depolarization on the OCT signal, an experimental solution based on a modified Mach-Zehnder interferometer [14-17] is proposed, (Fig. 2), involves the introduction of additional optical element polarization modulator (PM), a feedback line to eliminate depolarization and the use of appropriate AI/ML methods for processing interference signals. The introduced PM operates in a quasi-static mode, without employing high-frequency switching. The polarization state is switched after each scan, within a time interval shorter than the eye's blink duration. Interference signal monitoring is performed digitally in two orthogonal channels.

The central processing unit (CPU) performs analysis of the amplitude components ratio. $(A_{\parallel} / A_{\perp})$. If the *x*-polarization at the input of the next lamella is altered, this will immediately result in an increase in the signal in vertical $(\parallel)$-channel. The use of a proportional–integral (PI) controller algorithm allows adjusting the voltage on the PM to a minimum $A_{\perp}$. All "modulation sensitivity" is implemented in software. Fast switching is ensured by using photodiodes with digital frame subtraction/addition, which eliminates the need for a separate hardware synchronizer. The timestamp of each frame and PM command is recorded by the same board. The photodetectors, combined with software analysis, act as a sensitive synchronous demodulator, enabling registration and compensation of the modulation effect without additional hardware complexity. Thus, in our implementation, the influence of the PM is detected directly through changes in the signal ratio in the orthogonal channels, and correction is performed via digital feedback. This approach to constructing the experimental setup significantly simplifies the optical scheme, reduces cost, and enables effective signal correction at up to 10 Hz PM of updating the spatial position of the PM.

The broadband light source (*L*), (Fig. 2), a Ti:sapphire laser, is characterized by a spectral half-width of 170 nm and a central wavelength λ_0 of 800 nm. For the anterior stroma of the refractive index *n*=1.38 [14-16], the longitudinal resolution will be 1.2 μm, which is sufficient for depth-resolved imaging of the stromal structure. Transverse scanning involves pixel-by-pixel analysis, defined by the scanning step and aligned with the transverse

resolution $\delta x, y = \sqrt{2\ln 2} \times [\lambda_0 / \pi NA]$ of the proposed OCT scheme. The numerical aperture NA determines the focal depth of the beam: $b = n\lambda_0 / 2\pi NA^2$ in the medium [14-16], which corresponds to the thickness of the studied sample up to 100 μm in the anterior stroma region. The condition for transverse scanning is the ability to analyze and evaluate the transverse dimensions of the lamella and keratocytes, which in this case is achieved by 28×28 scans within a 200 μm×200 μm analyzed area.

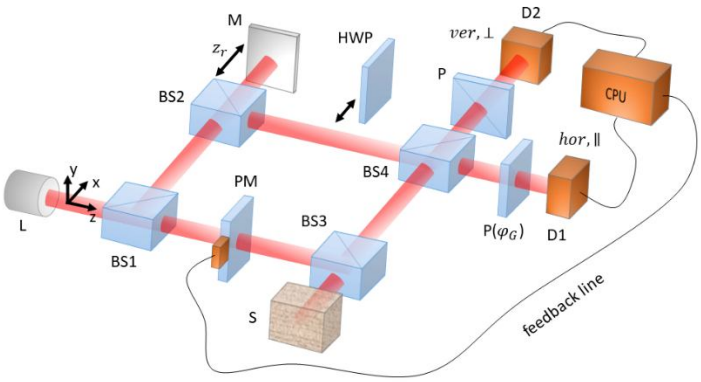

Fig. 2. The modified Mach-Zehnder interferometer scheme: L – radiation source; BS1, BS2, BS3, BS4 – nonpolarizing beamsplitters; M – mirror; HWP – half-wave plate; D1, D2 – photodetectors; CPU – central processing unit; $P(\varphi_G)$ – polarizer in the horizontal channel allowing to restore the initial horizontal polarization of the beam, which makes it possible to estimate the geometric phase; P – polarizer in the vertical channel, allowing to recover the vertical component of the signal; PM – polarization modulator; S – sample. x, y, z – laboratory coordinate frame, connected with the beam propagation direction.

The essence of the proposed experimental model is that a horizontal linear polarization is recovered in the horizontal channel behind the polarizer $P(\varphi_G)$ It repeats the polarization state in front of BS1 at the input of the interferometer (Fig. 2). The intensity measurement is carried out in both horizontal ($hor, \parallel$) and vertical ($ver, \perp$) channels of the interferometer. Information about two orthogonal components (intensity, amplitude, and phases) of the object beam is extracted from the horizontal and the vertical arms of the interferometer.

The nonpolarizing beamsplitters (BS1-BS4) perform the function of dividing the intensity of the incident beam in the transmission and reflection directions in the ratio of 50/50, equally redistributing the beams through the two channels. In order to extract information from the interference signal about the phase delay δ (or dynamic phase), determined by the object thickness, it is required to have y-components of the superimposing beams. For this purpose, we introduce an additional half-wave plate HWP, placing it in front of the beamsplitter BS4, and analyze the signal by the detector D2. The plate is oriented in such a way as to form an angle of 45° between the fast axis of the HWP and the horizontal direction.

The interference signals in the horizontal ($hor, \parallel$) and vertical ($ver, \perp$) channels of the interferometer (Fig. 3) can be expressed as [14-16]:

$$I_{hor,\,ver}(z_r) = I_r + I_{\parallel,\perp} + 2A_r \sum_{i=1}^{N_d} A_{\parallel,\perp_i} \cos\left(\varphi_{\parallel,\perp_i} - \varphi_0\right) \Gamma(z_r). \quad (4)$$

Here A_r, φ_0 – amplitude module and phase of the reference wave, z_r – optical path length in the reference arm, $\Gamma(z_r)=\exp\left(-\left[(2z_r-L_i)/l_c\right]^2\right)$ – coherence function, L_i – optical path length of the i-th photon packet in the medium. $A_{\|,\perp_i}$ - amplitude components (horizontal ($hor,\|$) and vertical ($ver,\perp$)) of one photon packet of the object signal, $\varphi_{\|,\perp}{}_i=\arg(\mathbf{E}_i)$ – phase components. $A_{\|}=\sum_{i=1}^{N_d}A_{\|}{}_i$, $A_{\perp}=\sum_{i=1}^{N_d}A_{\perp}{}_i$ – available from the interference-pattern envelopes in the $hor,\|$ - and $ver,\perp$ -channels of the interferometer.

$\mathbf{E}_i=\begin{pmatrix}E_{\|i}\\E_{\perp i}\end{pmatrix}=\begin{pmatrix}A_{\|_i}\exp\left(i\varphi_{\|_i}\right)\\A_{\perp_i}\exp\left(i\varphi_{\perp_i}\right)\end{pmatrix}$ - Jones vector of a single photon packet at the output from the medium, taking into account the signal modification due to birefringence in the lamella, scattering in the epithelium, spatial localization of keratocytes, and depolarization of the photon packet. $l_c=\frac{2\ln 2}{\pi n}\frac{\lambda^2}{\Delta\lambda}$ – the coherence length in a medium of refractive index n determines the longitudinal resolution $\delta z=l_c$ and specifies the thickness of the optical material, i.e., the number of lamellae that can be resolved separately. We assume that 8 photon packets are distributed within one pixel. Phase information is contained in the high-frequency component $\cos\left(\varphi_{\|,\perp}{}_i-\varphi_0\right)$.

Information about the geometric internal structure of the birefringent lamella, embedded in the refinement of the orientation of collagen fibers, can be obtained from the analysis of the phase argument extracted from the intensity distribution in the horizontal ($hor,\|$) channel [1,14-16], as

$$\varphi_{hor}=\varphi_{\|}-\varphi_0=\pi+\varphi_D+\varphi_G-\varphi_0. \tag{5}$$

Here $\varphi_D=2\delta$ – dynamic phase, $\varphi_G=\arctan\left(\tan\gamma\cos 2\alpha\right)$ – geometric phase, which is determined by the spatial structure of the birefringent medium. The orientation of the optical axis in the x-y plane is specified by the azimuthal angle α, the parameter of the model estimation.

Phase retardation $\gamma= kd\,(n_e-n_o)$ defines the quantity associated with the birefringent properties of an anisotropic medium.

Information about the dynamic phase can be obtained by analyzing the interferogram from the vertical ($ver,\perp$) arm, with a phase φ_{ver} between the superimposing components:

$$\varphi_{ver}=\frac{\pi}{2}+\varphi_D-\varphi_0. \tag{6}$$

To obtain phase information, i.e., information about $\varphi_{hor(ver)}$, with a subsequent transition to extracting data about γ and α, ready-made software solutions proposed in *Mathematica* are used. In this case, it is sufficient to discretize the obtained intensity distribution (Fig. 3), to which the Hilbert transform has been applied, enabling the transition to $\varphi_{hor(ver)}$ (Fig. 4a).

This approach can be considered an alternative software solution for the task of phase $\varphi_{hor(ver)}$ information recovery from interferograms, as opposed to the semi-empirical, graphical method described and implemented in [14-16].

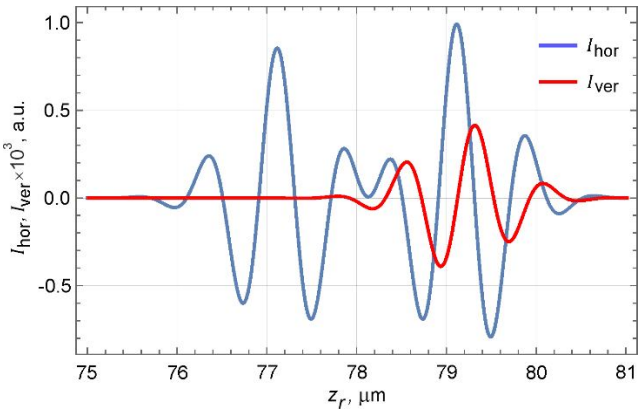

Fig. 3. Resulting interference signals in the horizontal ($hor,\|$) and vertical ($ver,\perp$) channels of the interferometer.

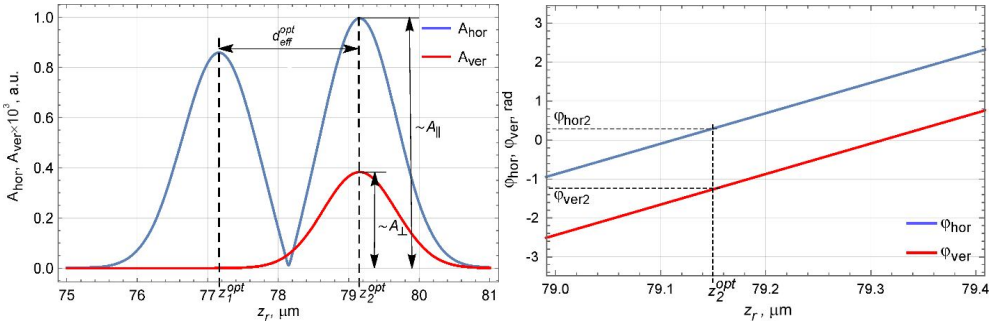

(a) (b)

Fig. 4. (a) Distribution of envelopes (A-scans) and (b) phase of the complex analytical signal for interferograms obtained in two channels of the interferometer. Here z_1^{opt} (z_2^{opt}) is the optical length of the signal path in the object arm, which is formed by reflection from the front (back) surface of the lamella, respectively, d_{eff}^{opt} is the effective optical thickness of the lamella, $\varphi_{hor(ver)}$ are the analytical-signal phases corresponding to reflection from the back surface of the lamella.

The known position of the envelope maxima in the horizontal channel for $z_{1,2}^{opt}$ makes it possible to determine the optical path length (the effective optical thickness of the lamella $d_{eff}^{opt} = z_2^{opt} - z_1^{opt} \equiv d_{eff}\bar{n}$) (Fig. 4a). The maximum value of the amplitude distribution $A_{hor,ver}\left(z_2^{opt}\right)$, evaluated for the inner surface, allows extraction of $A_{\|,\perp}$ (Fig. 4a). Accordingly, for $z_{1,2}^{opt}$, from the vertical channel, the phase value (Fig. 4b) $\varphi_{hor2,ver2} = \varphi_{hor,ver}\left(z_2^{opt}\right)$, defines the dynamic phase $\varphi_D = \varphi_{ver2} + \varphi_0 - \pi/2$, while the phase difference in two channels $\varphi_G = \varphi_{hor2} - \varphi_{ver2} + \pi/2$ represents the geometric phase. The angle of deviation of the slow axis of the lamella (orientation of collagen fibers) is β from the vertical direction ($\beta = 0$ when the slow axis is oriented along the z axis and $\beta = 90°$

when it oriented in the horizontal plane) and is also a factor influencing the magnitude of the birefringence of lamella. In the laboratory coordinate system $\Delta n(\beta) = n(\beta) - n_o$, where $n(\beta) = n_o n_e / \sqrt{n_e^2 \cos^2\beta + n_o^2 \sin^2\beta}$ [22]. If the values of n_o, n_e are known, as well as the values of the birefringence of the medium (or the refractive index), then the angle β can be estimated from the analysis of the dependencies $n(\beta)$ or $\Delta n(\beta)$.

Thus, the above-described approach allowed for the recovery of the lamella parameters, i.e., the average refractive index $\overline{n} = 1.37248$, the effective thickness $d_{eff} = 1.4527$ μm, the phase delay $\gamma = 0.00554$ rad, the angle $\alpha = 52.55°$, the birefringence $\Delta n(\beta) = 5.1456 \times 10^{-4}$ and the angle $\beta = 75.3°$. In this case, the relative errors in the obtained parameters are: $\varepsilon_\alpha = 1.86\%$, $\varepsilon_\beta = 1.46\%$, $\varepsilon_\gamma = 4.97\%$, $\varepsilon_{\overline{n}_i} = 0.173\%$, $\varepsilon_{\Delta n} = 0.86\%$, $\varepsilon_{deff} = 0.17\%$.

The final stage of modeling involves the restoration of the structure of the eye cornea, taking into account the distribution of keratocytes along the lamella structure by assessing the scattered radiation generated by keratocytes (Fig. 5). The geometric thickness of the layers is defined as $d = d_{opt} / n$. The 2D-OCT result in x-z plane is presented in real scales of the object thickness d for its central part (diameter is about 5 mm) (Fig. 5). The inset, marked by red, highlights a region within the full width at half maximum of the focused beam, approximately 7 μm in the transverse *x*-direction and about 40 μm in the longitudinal *z*-direction.

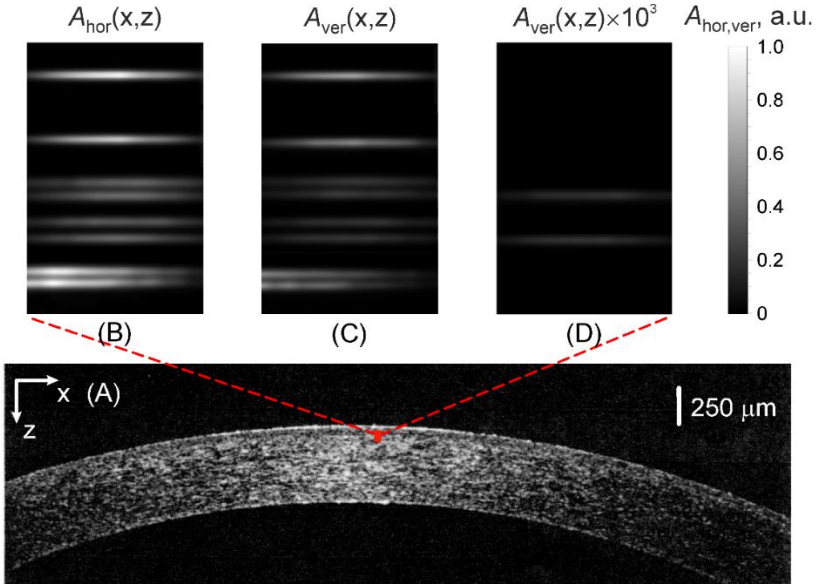

Fig. 5. The OCT restored signal - (A). Two-dimensional distributions of the analytical-signal amplitudes (B-scans) in the horizontal (*hor*,||) – (B) and vertical (*ver*,⊥) – (C) channels. (D) displays the "pure" contribution of the ⊥-polarization associated exclusively with the birefringence of the lamella in the vertical channel. The signal level is gray-scale color-coded, see the colorbar.

The insets (B)-(C) of Fig. 5 present the two-dimensional distribution of envelopes $A_{hor,ver}$ (*A*-scans, Fig. 4a) in the horizontal and vertical detection channels, forming a B-scan within the beam cross-section. Each *B*-scan contains 14 *A*-scans in the transverse *x*-direction. The signal within each pixel is summarized by the number of photons, sequentially depicting Bowman's layer (disordered collagenous tissue layer between epithelium and stroma), two

lamellae, and a keratocyte (from top to bottom). The signal in the vertical channel arises due both to depolarization within the medium and lamella birefringence.

The inset (D) of the figure displays the "pure" contribution of the ⊥-polarization in the vertical channel, caused solely by birefringence (with approximately three orders of magnitude weaker compared to the horizontal component).

4. Conclusion

The presented work builds on and expands the ideas introduced in our previous study [1], which focused on improving the sensitivity of PS-OCT. This study aims to reconstruct the geometric and optical structure of the cornea using a modified Mach–Zehnder interferometer. By accounting for scattering centers, such as epithelial nuclei–which cause radiation depolarization–we can present a more complete OCT image with better structural reproduction, achieving a 22.84% increase in accuracy. The experimental setup, which includes an extra polarization modulator and a feedback line in the modified Mach–Zehnder interferometer, allows control over the linear horizontal polarization state of the incident beam as it interacts with each lamella. Removing the "noisy" vertical component of the object signal caused by depolarization improves the longitudinal resolution of the PS-OCT method. Additionally, pixel-by-pixel scanning within the beam aperture enables polarization control at each pixel, which enhances the transverse resolution.

Funding. This research was funded by Taizhou Research Institute of Zhejiang University, Taizhou, China.

Conflict of interest. The authors declare no conflicts of interest.

Acknowledgment. This publication was supported by National Research Foundation of Ukraine (NRFU), project No. 2025.06/0086 'Innovative Methods and Systems of Laser Communication in Turbulent Atmospheric Environments Based on Phase Singularities'

References

1. Angelsky, O. V., Zenkova, C. Y., Ivanskyi, D. I., & Ursuliak, Y. (2025). Monte Carlo Model for Describing Photon Interactions with Biological Tissue in New Approaches of Polarization-Sensitive Optical Coherence Tomography. *Optical Memory and Neural Networks*, *34*(1), 30-48.
2. Torzicky, T. (2014). *Polarization sensitive optical coherence tomography at 1060 nm for retinal imaging*. [Unpublished doctoral dissertation]. Medical University of Vienna.
3. Hee, M. R., Huang, D., Swanson, E. A., & Fujimoto, J. G. (1992). Polarization-sensitive low-coherence reflectometer for birefringence characterization and ranging. *Journal of the Optical Society of America B*, *9*(6), 903-908.
4. Götzinger, E., Pircher, M., & Hitzenberger, C. K. (2005). High speed spectral domain polarization sensitive optical coherence tomography of the human retina. *Optics Express*, *13*(25), 10217-10229.
5. Baumann, B. (2017). Polarization sensitive optical coherence tomography: a review of technology and applications. *Applied Sciences*, *7*(5), 474.
6. Pierce, M. C., Shishkov, M., Hyle Park, B., Nassif, N. A., Bouma, B. E., Tearney, G. J., & De Boer, J. F. (2005). Effects of sample arm motion in endoscopic polarization-sensitive optical coherence tomography. *Optics Express*, *13*(15), 5739-5749.
7. Adie, S. G., Hillman, T. R., & Sampson, D. D. (2007). Detection of multiple scattering in optical coherence tomography using the spatial distribution of Stokes vectors. *Optics Express*, *15*(26), 18033-18049.
8. Schmitt, J. M., & Knüttel, A. (1997). Model of optical coherence tomography of heterogeneous tissue. *Journal of the Optical Society of America A*, *14*(6), 1231-1242.
9. Pan, Y., Birngruber, R., & Engelhardt, R. (1997). Contrast limits of coherence-gated imaging in scattering media. *Applied Optics*, *36*(13), 2979-2983.
10. Yadlowsky, M. J., Schmitt, J. M., & Bonner, R. F. (1995). Multiple scattering in optical coherence microscopy. *Applied Optics*, *34*(25), 5699-5707.
11. Yura, H. T., & Thrane, L. (2002, May). The effects of multiple scattering on axial resolution in optical coherence tomography. In *Summaries of Papers Presented at the Lasers and Electro-Optics. CLEO'02. Technical Diges* (pp. 476-vol). IEEE.
12. Lu, Q., Gan, X., Gu, M., & Luo, Q. (2004). Monte Carlo modeling of optical coherence tomography imaging through turbid media. *Applied Optics*, *43*(8), 1628-1637.
13. Zhu, L., Makita, S., Tamaoki, J., Zhu, Y., Mukherjee, P., Lim, Y., Kobayashi, M. & Yasuno, Y. (2023). Polarization-artifact reduction and accuracy improvement of Jones-matrix polarization-sensitive optical coherence tomography by multi-focus-averaging based multiple scattering reduction. *Biomedical Optics Express*, *15*(1), 256-276.

14. Angelsky, O. V., Bekshaev, A. Y., Zenkova, C. Y., Ivanskyi, D. I., Zheng, J., & Chumak, M. M. (2023). Modeling of the high-resolution optical-coherence diagnostics of bi-refringent biological tissues. *Frontiers in Physics*, *11*, 1260830.
15. Zenkova, C. Y., Angelsky, O. V., Ivanskyi, D. I., & Chumak, M. M. (2023). Geometric phase for investigation of nanostructures in approaches of polarization-sensitive optical coherence tomography. *Physics and Chemistry of Solid State*, *24*(4), 729-734.
16. Zenkova, C. Y., Ivanskyi, D. I., Diachenko, M., & Chumak, M. M. (2024, January). Model of optical axis orientation estimation in birefringent biological tissues. In *Sixteenth International Conference on Correlation Optics* (Vol. 12938, pp. 39-42). SPIE.
17. Zenkova, C., Angelsky, O., & Ivanskyi, D. (2024). New possibilities of polarization-sensitive optical coherence tomography using geometric phase approach for diagnostics of thin surface (subsurface) biological layers. *Optica Applicata*, *54*(3).
18. Gangnus, S. V., Matcher, S. J., & Meglinski, I. V. (2004). Monte Carlo modeling of polarized light propagation in biological tissues. *Laser Physics*, *14*(6), 886-891.
19. Tuchin, V. V. (2015). *Tissue optics: Light scattering methods and instruments for medical diagnosis* (3rd ed.). SPIE Press.
20. Collett, E. (2005). *Field guide to polarization*. SPIE Press.
21. Meglinski, I., Kirillin, M., Kuzmin, V., & Myllylä, R. (2008). Simulation of polarization-sensitive optical coherence tomography images by a Monte Carlo method. *Optics Letters*, *33*(14), 1581-1583.
22. Tuchin, V. V. (2016). Polarized light interaction with tissues. *Journal of Biomedical Optics*, *21*(7), 071114-071114.
23. Lee, G. D. R., Kim, D. H., Kwon, et al. (2023, December). A 0.5 μm pixel 3-layer stacked CMOS image sensor with deep contact and in-pixel Cu-Cu bonding technology. In *2023 International Electron Devices Meeting (IEDM)* (pp. 1-4). IEEE.
24. Lopez-Mago, D., Canales-Benavides, A., Hernandez-Aranda, R. I., & Gutiérrez-Vega, J. C. (2017). Geometric phase morphology of Jones matrices. *Optics Letters*, *42*(14), 2667-2670.
25. Lippok, N., Coen, S., Leonhardt, R., Nielsen, P., & Vanholsbeeck, F. (2012). Instantaneous quadrature components or Jones vector retrieval using the Pancharatnam–Berry phase in frequency domain low-coherence interferometry. *Optics Letters*, *37*(15), 3102-3104.

O. V. Angelsky, C. Yu. Zenkova, A. Ya. Bekshaev, D. I. Ivanskyi, M. Diachenko, Jun Zheng, Xinzheng Zhang. (2025). New Solutions for Polarization-Sensitive Optical Coherence Tomography**.** *Ukrainian Journal of Physical Optics*, *26*(3), 03067 – 03077.
doi: 10.3116/16091833/Ukr.J.Phys.Opt.2025.03067.

Анотація. *Робота є продовженням досліджень, представлених у [1], з реконструкції структури рогівки ока на базі модифікованого інтерферометра Маха-Цендера, з додатковим поляризаційним модулятором та лінією зворотного зв'язку. Відмінною особливістю цього підходу є врахування деполяризації об'єктного сигналу, що виникає внаслідок розсіювання на епітеліальних клітинах і кератоцитах рогівки. Введене співвідношення між поляризованою та деполяризованою компонентами інтенсивності зареєстрованого об'єктного сигналу дозволило оцінити вплив деполяризації на сигнал, а запропоноване експериментальне рішення дало змогу підвищити точність реконструкції структури ока на 22,84%. Як показано у запропонованому дослідженні, усунення «шумової» вертикальної компоненти об'єктного сигналу, спричиненої деполяризацією вхідної горизонтально лінійно поляризованої хвилі, забезпечило успішну реконструкцію структури рогівки за даними, отриманими у вертикальному каналі інтерферометра.*

Ключові слова*: оптична когерентна томографія, деполяризація, центри розсіювання, подвійне променезаломлення, метод Монте-Карло, інтерферометр Маха-Цендера*